Impedance-Near-Zero Acoustic Metasurface for Hypersonic Boundary-Layer Flow Stabilization

Rui Zhao,[1] Tuo Liu,[2,3,*] Chih-yung Wen,[2,†] Jie Zhu,[2,3,‡] and Li Cheng[2]

[1]*School of Aerospace Engineering, Beijing Institute of Technology, Beijing 100081, China*
[2]*Department of Mechanical Engineering, The Hong Kong Polytechnic University, Kowloon, Hong Kong Special Administrative Region*
[3]*The Hong Kong Polytechnic University Shenzhen Research Institute, Shenzhen 518057, China*

Hypersonic boundary-layer transition induced by the Mack second mode is a fundamental issue in fluid mechanics and hypersonic vehicle design, whose physics are not yet fully understood. Nevertheless, given the acoustic nature of the Mack second mode, ultrasonic absorptive coatings have been proposed to dissipate the wave energy and thus stabilize the hypersonic boundary-layer flow. We, however, show that even with little damping, the Mack second mode can be greatly suppressed by introducing an artificial boundary of near-zero surface acoustic impedance. This phenomenon can be attributed to the minimized acoustic pressure perturbation at the antinode of the Mack second mode, which prevents the surface-wavelike mode from being effectively excited. As a practical realization, we present a grooved acoustic metasurface and numerically verify its feasibility. Results reveal that the out-of-phase behavior between the incident and reflected waves at the resonant frequency minimizes the near-surface acoustic pressure, largely inhibiting the growth of the Mack second mode. Our study sheds light on the physical mechanism of the Mack second mode and opens up alternative possibilities toward full control of hypersonic boundary-layer transition with acoustic metasurfaces.

I. INTRODUCTION

In a hypersonic and low-disturbance environment, transition from laminar to turbulent flow along a smooth surface occurs as a result of the amplification of unstable boundary-layer modes, and its initial phase is associated with the excitation and amplification of the first and/or Mack second mode [1–5]. For relatively cooling wall conditions (less than a factor of 0.2 of the adiabatic wall temperature), the first mode is strongly stabilized, whereas the Mack second mode remains unstable and triggers an early transition [6]. In practice, such a transition generates significant increases in viscous drag and heat flux, leading to severe restrictions on the performance and thermal protection system of hypersonic vehicles. Delaying the transition and maintaining a laminar boundary layer as long as possible guarantee better fuel efficiency and lower drag and heat flux.

Although the mechanism behind the complex physical process has not yet been entirely clarified [5], it is known that the Mack second mode behaves like a trapped acoustic mode propagating in a waveguide between the wall and the sonic line, but with phase velocity higher than the speed of sound, as illustrated in Fig. 1. Each time an acoustic wave is reflected at the sonic line, it changes from a compression wave to an expansion wave and vice versa. The longitudinal wavelength of the Mack second mode is about twice the boundary-layer thickness, and its frequency reaches hundreds of kHz corresponding to the ultrasonic band [8].

As the Mack second mode exhibits acoustic-wavelike behavior, one straightforward way to suppress its development while minimally disturbing the mean flow is to dissipate the acoustic wave energy by implementing an absorptive boundary [5,6]. Following this idea, a so-called ultrasonic absorptive coating (UAC) was proposed and optimized to obtain the required dissipation effect through the thermal and viscous boundary layers inside the narrow cavities [9–12]. Contrary to this intuitive thinking, here we show that an effective boundary with hardly any absorptive capability can still suppress the Mack second mode provided that its surface acoustic impedance approaches zero. The performance is even improved over that of the absorptive boundary. In the following, we first discuss the underlying physics of the observed abnormal phenomenon, and then demonstrate a practical realization of such an impedance-near-zero boundary based on the concept of acoustic metasurfaces [13–30].

_____

*tuo.liu@connect.polyu.hk
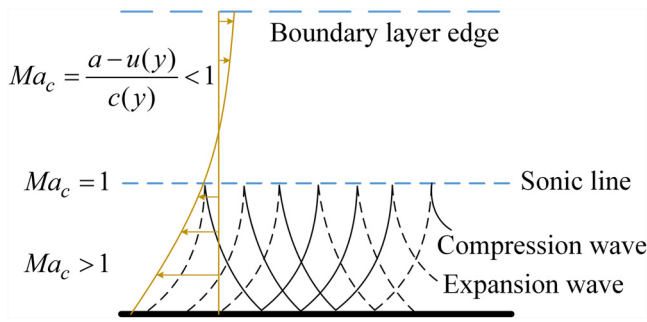†chihyung.wen@polyu.edu.hk
‡jiezhu@polyu.edu.hk

FIG. 1. Acoustic modes trapped in the relative supersonic region where the convective Mach number $Ma_c > 1$, stationary in this frame of reference, adapted from Morkovin Ref. [7]. Here, $u(y)$ and $c(y)$ denote the local speed of flow and sound, respectively, and a denotes the disturbance phase speed.

II. THEROTICAL ANALYSIS

For hypersonic boundary-layer flow problems [9–12, 31], the boundary condition at the wall surface is generally modeled as $v'_w = p'_w/Z$, where v'_w and p'_w are the vertical flow velocity and acoustic pressure at the wall, respectively. Z is the surface acoustic impedance, which depends on the properties of the wall material, mean flow characteristics at the wall surface, and flow-perturbation parameters such as wave frequency [31]. Z becomes infinite for a rigid wall and is often designed to match the specific acoustic impedance of the background medium to maximize the absorption effect [11,12]. Note that, as a trapped mode within a waveguide, the sound ray of the Mack second mode is almost normal to the wall surface [32], which means the absorption reaches a maximum for the matched impedance. The stability characteristics of hypersonic boundary layers can be theoretically evaluated using linear stability analysis theory (LST) [1]. We consider a two-dimensional perturbation flow field $q'(x,y,t)$, which takes the form of a wavelike perturbation function

$$q'(x,y,t) = \hat{q}(y)\exp[i(\alpha x - \omega t)], \quad (1)$$

where $\hat{q}(y)$ is a complex amplitude function, α denotes the dimensionless wavenumbers, and ω denotes the angular frequency. For spatial stability, the frequency ω is real, whereas α is a complex eigenvalue with $\alpha = \alpha_r + i\alpha_i$. If $\alpha_r > 0$ and $\alpha_i < 0$, the flow is unstable with spatial growth rate $-\alpha_i$ and streamwise wavenumber α_r. In our theoretical modeling, as depicted in Fig. 2(a), a slot of periodic suction blowing at a fixed frequency of $f = 138.74$ kHz is introduced at the beginning of the surface. At this frequency, the typical Mack second mode will be excited along the second half of the surface [8]. The surface is 0.2-m long with an isothermal wall temperature of $T_w = 293$ K. Its first half is rigid, and an impedance boundary condition is implemented along the second half [highlighted

area in Fig. 2(a)], in which we define a normalized surface acoustic impedance $Z^* = Z/Z_0$, where Z_0 is the background flow impedance. The freestream conditions are as follows: Mach number $Ma_\infty = 6.0$, unit Reynolds number $Re_\infty = 1.05 \times 10^7$ m^{-1}, and temperature $T_\infty = 43.18$ K. As mentioned above, the maximum sound absorption corresponds to the matched surface acoustic impedance, namely, $Z^* = -1$, suggesting the most prominent dissipation of the Mack second mode. As shown in Fig. 2(b), by varying the surface impedance from $Z^* \to -\infty$ (rigid) to $Z^* = -2$ and $Z^* = -1$, the growth rate of the Mack second mode is indeed largely reduced. Surprisingly, the growth rate continues to decrease as Z^* approaches zero. In other words, the boundary tends to become nondissipative, yet the Mack second mode can still be effectively suppressed in an even better manner. This is not in line with our conventional physics understanding of hypersonic boundary-layer stabilization.

Actually, our findings can be evidently explained by examining the pressure distributions of the Mack second mode using a high-order accurate direct numerical simulation (DNS) [8,12]. As shown in the upper subplot of Fig. 3(a), a typical Mack second mode (two-cell structure) is formed when the perturbation propagates downstream along a rigid surface. This is similar to a surface acoustic mode confined to the interface and evanescent along the vertical direction. The amplitude of its
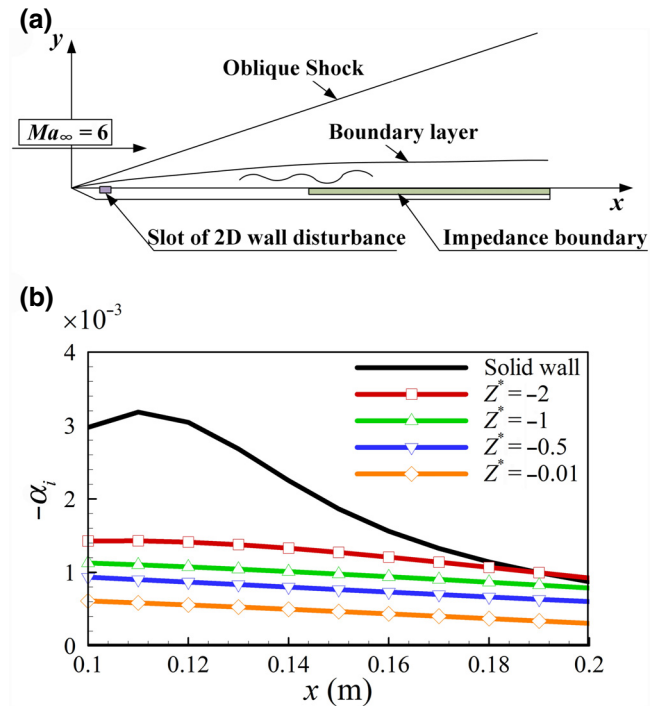

FIG. 2. Linear stability analysis of hypersonic boundary-layer flow along an impedance boundary. (a) Schematic drawing of problem formulation. (b) Growth rate distributions of the Mack second mode for different surface impedance values.
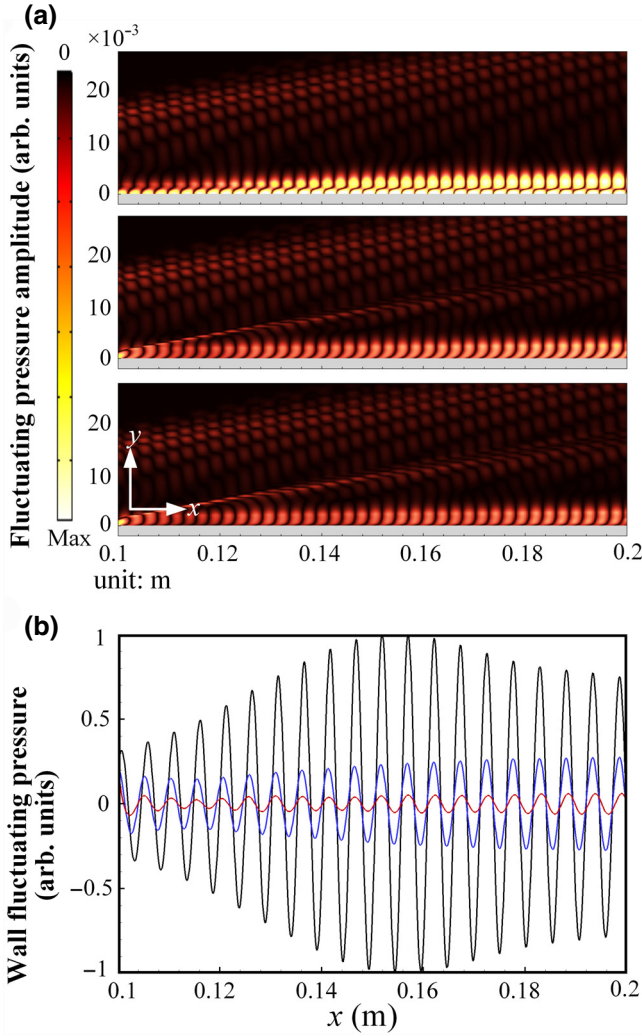
(a)

(b)

FIG. 3.   Direct numerical simulation of the fluctuating pressure field in the hypersonic flow. (a) Fluctuating pressure amplitude contours for the rigid boundary $Z^* \rightarrow -\infty$ (upper), the absorptive boundary $Z^* = -1$ (middle), and the impedance-near-zero boundary $Z^* = -0.01$ (lower). (b) Comparison of fluctuating pressure distributions for different boundary conditions: black, rigid; blue, $Z^* = -1$; red, $Z^* = -0.01$. All curves are normalized to the maximum fluctuating pressure over the rigid boundary.

pressure perturbation reaches a maximum at the surface, corresponding to an antinode. An absorptive boundary efficiently dissipates the acoustic wave energy because of the small angle of incidence, but cannot fully eliminate the Mack second mode as the flow field keeps offering energy to the boundary layer [32] [middle subplot of Fig. 3(a)]. In contrast, the impedance-near-zero boundary forces the acoustic pressure fluctuation at the antinode to approach zero [lower subplot in Fig. 3(a)]. According to the relation $Zv'_w = p'_w$, the excitation of the Mack second mode is fundamentally suppressed. In this case, the pressure perturbation in the hypersonic flow field can no longer be

effectively coupled into the Mack second mode. As can be seen in Fig. 3(b), the pressure fluctuation above the impedance-near-zero boundary (red line) is much weaker than that of the absorptive boundary (blue line).

III. PRACTICAL REALIZATION WITH ACOUSTIC METASURFACE

Despite the potential of an impedance-near-zero boundary to stabilize the hypersonic boundary layer flow, realizing it with traditional materials and structures is extremely challenging. The recent emergence of acoustic metasurfaces [13–30] provides a practical way to bring such an unusual artificial boundary condition to life. Acoustic metasurfaces are planar metamaterial structures constructed with monolayer or multilayer stacks of subwavelength building blocks, which have significantly broadened the horizon of acoustic wave manipulation from wave-front modulation [13–16,18,19,24,26,27], to sound insulation and absorption [17,20,22], and so on. Among the wide variety of unconventional functionalities, effective impedance engineering enabled by acoustic metasurfaces [14,22,25,28–30] makes it possible to tune the boundary impedance to near zero for the above-mentioned hypersonic boundary layer problem. In order to validate our idea unambiguously, here, we consider the simplest structural design: a rigid surface periodically corrugated with subwavelength grooves. As Fig. 4(a) shows, the acoustic metasurface extends to infinity in the x and z directions. The half-width and depth of the cavities are b and H, respectively, with the unit-cell period being s. The porosity and aspect ratio are $\phi = 2b/s$ and $A_r = 2b/H$, respectively. Assuming that the periodicity s is much smaller than the acoustic wavelength λ_{acs}, the plane wave expansion method [12,29,30] can be used to derive the normalized effective surface acoustic impedance of the proposed metasurface as

$$Z^* = \frac{1}{\rho_w c_w} \left. \frac{p}{v} \right|_{y=0}$$

$$= 1 + \frac{1}{j \tan(k_c H)\phi \frac{\rho_w}{\tilde{\rho}} \frac{k_c}{k_0}} - \sum_{n=-\infty}^{+\infty} \frac{k_0}{\sqrt{k_0^2 - \left(\frac{2\pi n}{s}\right)^2}} S_n^2, \tag{2}$$

where ρ_w, c_w, and $k_0 = \omega/c_w$ are the local density, speed of sound, and wavenumber at the wall, respectively; $\tilde{\rho}$ and k_c are the complex dynamic density and wavenumber inside the cavity [12]. $S_n = \mathrm{sinc}(k_x b + \phi \pi n)$ is the overlap integral between the nth-order diffracted mode and the fundamental mode inside the cavity, where k_x is the parallel momentum. At the resonance frequency, Z^* is a purely real number governed by the geometrical parameters of the unit cell as well as the viscosity and thermal conductivity inside the cavities. Note that,
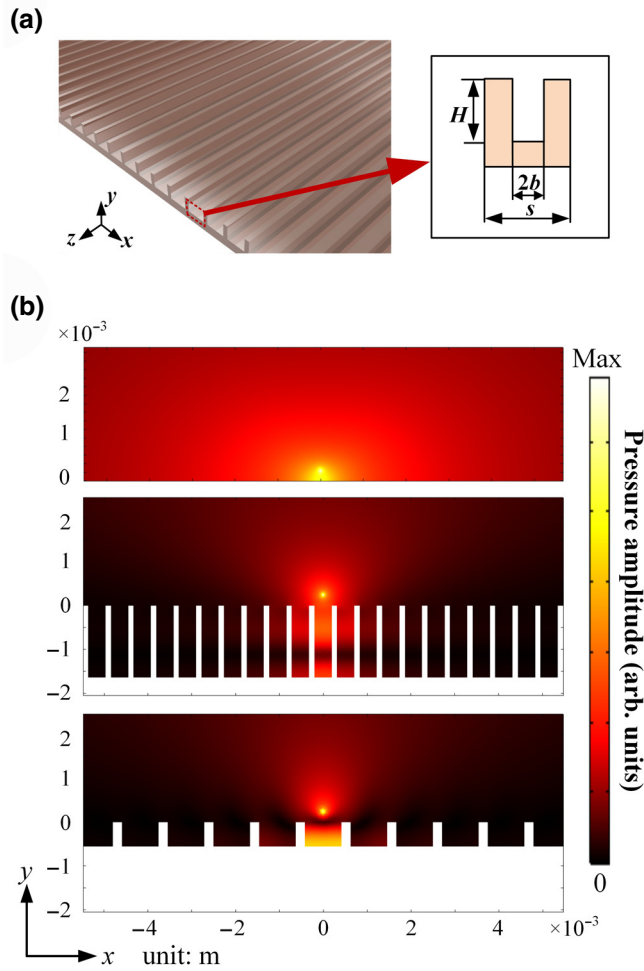
FIG. 4. Acoustic metasurface with subwavelength grooves. (a) Schematic illustration of the metasurface. (b) Simulated absolute acoustic pressure fields for different types of surfaces in the absence of hypersonic fluid flow. Upper: rigid surface; middle: absorptive metasurface with matched impedance $|Z^*| = 1$ and the corresponding shape parameters $\phi = 0.76$, $A_r = 0.24$, and $b = 1.96 \times 10^{-4}$ m, lower: impedance-near-zero metasurface with $|Z^*| = 0.15$ and the corresponding shape parameters $\phi = 0.8$, $A_r = 1.5$, and $b = 4.16 \times 10^{-4}$ m. During all simulations, a point sound source is located at $y = 2.48 \times 10^{-4}$ m (one-tenth of the incident wavelength) and immersed in the quiescent air of density $\rho_w = 5.59 \times 10^{-3}$ kg/m³ and speed of sound $c_w = 343.11$ m/s, with the operating frequency being 138.74 kHz. The above ρ_w and c_w are equal to the flow parameters at wall location $x = 0.15$ m from steady flow calculation.

despite the nonzero nature of Z^* in a passive system (owing to the inherent viscothermal losses), we may still obtain a relatively low value of Z^* through a careful selection of the geometrical parameters. To this end, a numerical optimization process [12] is applied to determine the geometrical parameters required by a near-zero surface acoustic impedance through solving Eq. (2) with program

loops in the following order: loop 1: $0.2 \le \phi \le 0.8$, loop 2: $0.06 \le A_r \le 1.5$, loop 3: $0 < f_{acs} < \min(\phi/A_r, 2.0)$, where $f_{acs} = fH/c_w$ is the normalized frequency.

Before taking into account the hypersonic fluid field, we perform full-wave finite element simulations to examine the acoustic characteristics of our design in the first place. As shown in the lower subplot of Fig. 4(b), the absolute acoustic pressure field generated by a near-surface point source is extremely weak at the interface $y = 0$, as a result of the out-of-phase behavior between the incident and reflected waves. Sound waves are localized within the central cavity and hardly transmit to neighboring ones, corresponding to a band gap of the surface acoustic wave. This is in stark contrast to the sound field of an impedance-matched metasurface [middle subplot of Fig. 4(b)], namely, an optimized UAC with $|Z^*| = 1$, in which most of the incident waves are absorbed compared with the case of a rigid surface [upper subplot of Fig. 4(b)], but the acoustic pressure oscillation at the interface remains strong.

With this carefully designed impedance-near-zero metasurface, the aforementioned stabilization problem of the two-dimensional hypersonic boundary-layer flow [Fig. 2(a)] is reconsidered by employing DNS to simulate the spatial development of perturbations that interact with the metasurface. The corresponding cavity shape parameters are as listed in the caption of Fig. 4, and the excitation source located in the left-hand side is a slot of periodic suction blowing at a fixed frequency of $f = 138.74$ kHz. Unlike the typical two-cell Mack second mode structures along the rigid surface [Fig. 5(a), upper subplot], the upper cells join the lower part when moving through the metasurface region ($x = 0.12$–0.18 m), and then separate to form the typical two-cell structures downstream beyond $x > 0.18$ m [Fig. 5(a), middle and lower subplots]. For the impedance-matched metasurface [Fig. 5(a), middle subplot], the trailing leg moves within the cavity. The intensity is greatly weakened due to the internal viscothermal dissipation. Whereas for the impedance-near-zero metasurface [Fig. 5(a), lower subplot], a minimum value appears as a result of the phase opposition of the instability waves at the surface, and the mode structure is divided in the cavity and above the surface [33]. The change in mode structures inhibits the amplification process of the Mack second mode. Figures 5(b) and 5(c) compare the fluctuating pressure distributions along the wall and the energy density spectrum at $x = 0.16$ m, respectively. Together, they confirm that the proposed impedance-near-zero acoustic metasurface can effectively suppress the Mack second mode instability, as predicted by our theoretical analysis. Compared with the optimized UAC (*viz.* the impedance-matched metasurface), the overall performance is slightly improved, and the shallow-cavity design would also be an advantage for manufacture and maintenance [5].
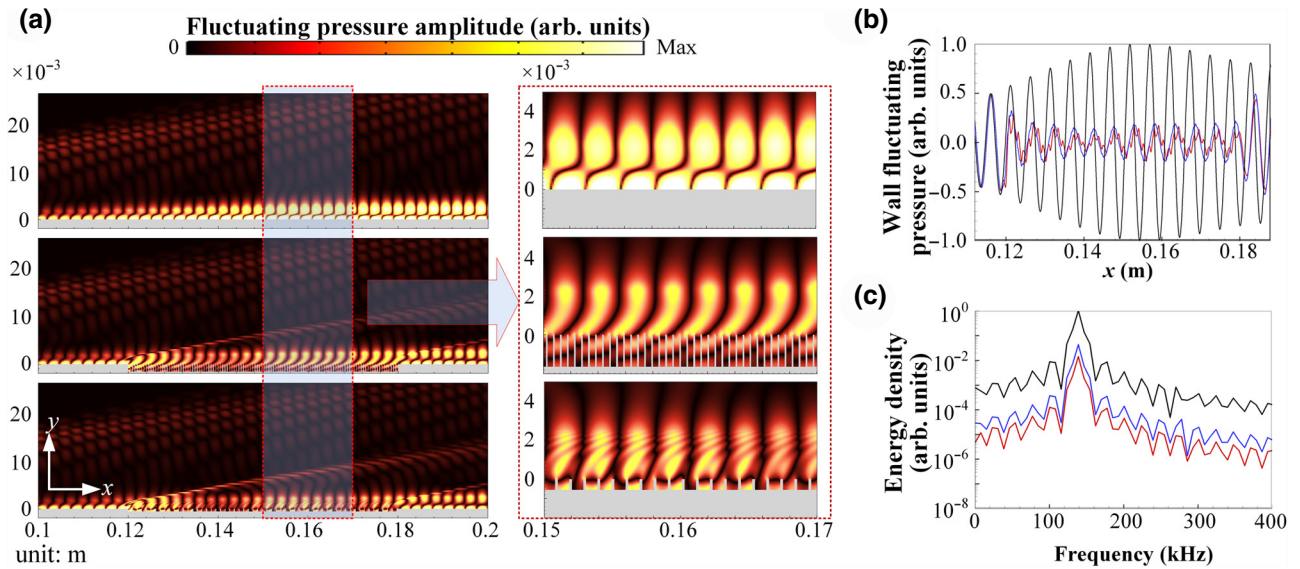
FIG. 5. Direct numerical simulation of fluctuating pressure fields when hypersonic flow passes the metasurface. Problem formulation is as for Fig. 2(a) except that the metasurface is only located at $x = 0.12$–0.18 m to save computational resources. (a) Fluctuating pressure amplitude contours for rigid boundary (upper), impedance-matched metasurface (middle), and impedance-near-zero metasurface (lower), with the corresponding zoomed-in views shown in the right column. (b) Comparisons of fluctuating pressure along the surface ($y = 0$) for different boundaries. (c) Comparisons of energy density at $(x, y) = (0.16$ m, 0 m) for different boundaries. In (b),(c), the black line represents data for the rigid boundary, the blue line for the impedance-matched metasurface, and the red line for the impedance-near-zero metasurface.

IV. CONCLUSION

To conclude, we demonstrate that an impedance-near-zero boundary is able to restrain the acoustic pressure perturbation at the antinode of the Mack second mode, and consequently stabilize the hypersonic boundary-layer flow. Contrary to the long-held belief that acoustic wave energy dissipation is indispensable in suppressing the Mack second mode, our result indicates that a nearly nondissipative boundary can effectively prevent this surface-wavelike mode from being generated. Using a well-designed acoustic metasurface, a practical realization of such impedance-near-zero boundary has been presented, in which a slightly improved performance is achieved compared with the optimized UAC. For more practical two-dimensional curved surfaces, such as hypersonic vehicles with a sharp cone configuration, we may readily replace the unit cell grooves with circular [29] or square [30] holes to achieve the same goal. On the other hand, the operating bandwidth could be broadened by introducing multiple resonances into the unit cell, which is an idea that has already been proposed to realize broadband and near-perfect sound absorption [34–36]. We believe the present study provides not only additional insights into the understanding of hypersonic transition mechanisms, but also an alternative paradigm for full control of hypersonic boundary-layer transition.

ACKNOWLEDGMENTS

[1] L. M. Mack, Boundary-layer stability theory, Jet Propulsion Lab Report No. 900-277. Rev. A, 1969; Transition and laminar instability, NASA Contract. Report No. 153203 (1977).

[2] E. Reshotko, Boundary-layer stability and transition, Annu. Rev. Fluid. Mech. **8**, 311 (1976).

[3] H. L. Reed and P. Balakumar, Stability of three-dimensional supersonic boundary layers, Phys. Fluids A **2**, 1341 (1990).

[4] M. V. Morkovin, E. Reshotko, and T. Herbert, Transition in open flow systems - a reassessment, Bull. Am. Phys. Soc. **39**, 1882 (1994).

[5] A. Fedorov, Transition and stability of high-speed boundary layers, Annu. Rev. Fluid. Mech. **43**, 79 (2011).

[6] A. V. Fedorov, A. N. Shiplyuk, A. A. Maslov, E. Burov, and N. D. Malmuth, Stabilization of a hypersonic boundary layer using an ultrasonically absorptive coating, J. Fluid Mech. **479**, 99 (2003).

[7] M. V. Morkovin, Transition at hypersonic speeds, NASA Contract. Report No. 178315 (1987).

[8] R. Zhao, C. Y. Wen, X. D. Tian, T. H. Long, and W. Yuan, Numerical simulation of local wall heating and cooling effect on the stability of a hypersonic boundary layer, Int. J. Heat Mass Transf. **121**, 986 (2018).

[9] A. V. Federov, N. D. Malmuth, A. Rasheed, and H. G. Hornung, Stabilization of hypersonic boundary layers by porous coatings, AIAA J. **39**, 605 (2001).

[10] X. Zhong and X. Wang, Direct numerical simulation on the receptivity, instability, and transition of hypersonic boundary layers, Annu. Rev. Fluid. Mech. **44**, 527 (2012).

[11] G. A. Brès, M. Inkman, T. Colonius, and A. V. Fedorov, Second-mode attenuation and cancellation by porous coatings in a high-speed boundary layer, J. Fluid Mech. **726**, 312 (2013).

[12] R. Zhao, T. Liu, C. Y. Wen, J. Zhu, and L. Cheng, Theoretical modeling and optimization of porous coating for hypersonic laminar flow control, AIAA J. **56**, 2942 (2018).

[13] Y. Li, B. Liang, Z. M. Gu, X. Y. Zou, and J. C. Cheng, Reflected wavefront manipulation based on ultrathin planar acoustic metasurfaces, Sci. Rep. **3**, 2546 (2013).

[14] J. Zhao, B. Li, Z. Chen, and C. W. Qiu, Manipulating acoustic wavefront by inhomogeneous impedance and steerable extraordinary reflection, Sci. Rep. **3**, 2537 (2013).

[15] Y. Xie, W. Wang, H. Chen, A. Konneker, B. I. Popa, and S. A. Cummer, Wavefront modulation and subwavelength diffractive acoustics with an acoustic metasurface, Nat. Commun. **5**, 5553 (2014).

[16] K. Tang, C. Qiu, M. Ke, J. Lu, Y. Ye, and Z. Liu, Anomalous refraction of airborne sound through ultrathin metasurfaces, Sci. Rep. **4**, 6517 (2014).

[17] G. Ma, M. Yang, S. Xiao, Z. Yang, and P. Sheng, Acoustic metasurface with hybrid resonances, Nat. Mater. **13**, 873 (2014).

[18] Y. Li, X. Jiang, R. Q. Li, B. Liang, X. Y. Zou, L. L. Yin, and J. C. Cheng, Experimental Realization of Full Control of Reflected Waves With Subwavelength Acoustic Metasurfaces, Phys. Rev. Appl. **2**, 064002 (2014).

[19] Y. Li, X. Jiang, B. Liang, J. C. Cheng, and L. K. Zhang, Metascreen-Based Acoustic Passive Phased Array, Phys. Rev. Appl. **4**, 024003 (2015).

[20] Y. Cheng, C. Zhou, B. G. Yuan, D. J. Wu, Q. Wei, and X. J. Liu, Ultra-sparse metasurface for high reflection of low-frequency sound based on artificial Mie resonances, Nat. Mater. **14**, 1013 (2015).

[21] X. Jiang, Y. Li, B. Liang, J. C. Cheng, and L. Zhang, Convert Acoustic Resonances to Orbital Angular Momentum, Phys. Rev. Lett. **117**, 034301 (2016).

[22] Y. Li and B. M. Assouar, Acoustic metasurface-based perfect absorber with deep subwavelength thickness, Appl. Phys. Lett. **108**, 063502 (2016).

[23] Y. Li, C. Shen, Y. Xie, J. Li, W. Wang, S. A. Cummer, and Y. Jing, Tunable Asymmetric Transmission Via Lossy Acoustic Metasurfaces, Phys. Rev. Lett. **119**, 035501 (2017).

[24] Y. F. Zhu, X. D. Fan, B. Liang, J. C. Cheng, and Y. Jing, Ultrathin Acoustic Metasurface-Based Schroeder Diffuser, Phys. Rev. X **7**, 021034 (2017).

[25] E. Bok, J. J. Park, H. Choi, C. K. Han, O. B. Wright, and S. H. Lee, Metasurface for Water-to-Air Sound Transmission, Phys. Rev. Lett. **120**, 044302 (2018).

[26] J. Li, C. Shen, A. Diaz-Rubio, S. A. Tretyakov, and S. A. Cummer, Systematic design and experimental demonstration of bianisotropic metasurfaces for scattering-free manipulation of acoustic wavefronts, Nat. Commun. **9**, 1342 (2018).

[27] Y. Zhu, J. Hu, X. Fan, J. Yang, B. Liang, X. Zhu, and J. Cheng, Fine manipulation of sound via lossy metamaterials with independent and arbitrary reflection amplitude and phase, Nat. Commun. **9**, 1632 (2018).

[28] L. Quan, X. Zhong, X. Liu, X. Gong, and P. A. Johnson, Effective impedance boundary optimization and its contribution to dipole radiation and radiation pattern control, Nat. Commun. **5**, 3188 (2014).

[29] L. Schwan, A. Geslain, V. Romero-Garcia, and J. P. Groby, Complex dispersion relation of surface acoustic waves at a lossy metasurface, Appl. Phys. Lett. **110**, 051902 (2017).

[30] T. Liu, S. Liang, F. Chen, and J. Zhu, Inherent losses induced absorptive acoustic rainbow trapping with a gradient metasurface, J. Appl. Phys. **123**, 091702 (2018).

[31] V. F. Kozlov, A. V. Fedorov, and N. D. Malmuth, Acoustic properties of rarefied gases inside pores of simple geometries, J. Acoust. Soc. Am. **117**, 3402 (2005).

[32] G. A. Brès, T. Colonius, and A. V. Fedorov, Acoustic properties of porous coatings for hypersonic boundary-layer control, AIAA J. **48**, 267 (2010).

[33] See the Supplemental Material http://link.aps.org/supplemental/10.1103/PhysRevApplied.11.044015, for the time evolution of fluctuating pressure fields obtained from DNS.

[34] T. Wu, T. J. Cox, and Y. W. Lam, From a profiled diffuser to an optimized absorber, J. Acoust. Soc. Am. **108**, 643 (2000).

[35] C. Zhang and X. H. Hu, Three-Dimensional Single-Port Labyrinthine Acoustic Metamaterial: Perfect Absorption with Large Bandwidth and Tenability, Phys. Rev. Appl. **6**, 064025 (2016).

[36] M. Yang, S. Y. Chen, C. X. Fuab, and P. Sheng, Optimal sound-absorbing structures, Mater. Horiz. **4**, 673 (2017).